Efficient BLACK-ICE Detection for Low Power Edge Devices

Mohammadreza Najafi, Saeid Gorgin, Mohammad K Fallah, Jeong-A Lee
Department of Computer Engineering, Chosun University, Gwangju, South Korea
najafi@chosun.kr, gorgin@chosun.ac.kr, mkfallah@chosun.ac.kr, jalee@chosun.ac.kr

***Abstract*—The modern idea of smart cities inspires urban planners and scholars to create a contemporary, secure, and sustainable infrastructure for citizens. Video surveillance cameras are installed to improve safety, but despite technological advancements, detecting anomalous events in surveillance videos remains challenging, often requiring significant human intervention. This study addresses this challenge by identifying objects of interest and utilizing openly accessible datasets for anomaly detection in video surveillance systems. A notable anomaly with severe implications is the presence of BLACK-ICE on highway surfaces. BLACK-ICE refers to a slender layer of ice that forms on road surfaces, diminishing the friction coefficient of the road. The presence of BLACK-ICE renders the road slippery, heightening the risk of safety incidents for both pedestrians and vehicles. Notably, identifying BLACK-ICE is challenging due to its transparent nature, distinguishing it from other slippery surfaces like wet or snowy roads. In this regard, Closed-Circuit Television (CCTV) systems deployed on highways emerge as a valuable tool for BLACK-ICE detection. Recognizing the time-sensitive nature of anomaly detection in computer vision applications, this research specifically focuses on investigating BLACK-ICE surface detection using edge devices. A novel method based on Convolutional Neural Network (CNN) and calculating sharpness and glossy factors of HSV format images has been introduced to enhance performance and optimize resource utilization without compromising accuracy.**

***Index Terms*—BLACK-ICE Detection, CCTV, HSV, CNN.**

I. Introduction

In recent years, the domains of machine learning (ML) and computer vision (CV) have undergone substantial development, playing a crucial role in addressing various complex challenges across diverse applications [1]. Through sophisticated processing and analysis, CV demonstrates the capacity to comprehend intricate details and acquire data at a profound level. Furthermore, these systems are designed to automate tasks analogous to those performed by the human visual system. Various multidisciplinary domains, including Automatic Inspection, Object Modeling, Process Control, Navigation, and Video Surveillance, actively employ CV [1].

Video surveillance has a significant application of CV, extensively utilized in both public and private settings for observation and monitoring purposes [2]. Intelligent video surveillance systems are deployed to autonomously identify, monitor, and analyze entities at an advanced level, eliminating the need for human intervention [3]. These systems find application in diverse settings such as homes, workplaces, hospitals, malls, and parking lots based on user preferences. The increasing deployment of surveillance cameras in public spaces, including roadways, intersections, banks, and shopping centers, aims to enhance public safety [4]. However, the monitoring capacities of law enforcement organizations have not kept pace, resulting in a noticeable disparity in camera usage, rendering the camera-to-human monitor ratio unsustainable [5].

A crucial aspect of video surveillance involves recognizing unusual events, such as traffic accidents, criminal activities, or illicit behavior. These anomalies occur less frequently than routine activities, emphasizing the need for intelligent computer vision algorithms to automatically detect video anomalies and reduce labor and time expenses. A notable anomaly on highways is the existence of icy road surface conditions, where annually in the United States, more than 116,800 individuals experience injuries in vehicle accidents on icy pavements, as indicated by the Federal Highway Administration [14]. Beyond the hazards posed by icy conditions, BLACK-ICE is identified as an even more perilous situation, frequently leading to accidents. The collision involving 69 vehicles on the Virginia Expressway in December 2019 and a traffic incident on the Yeongcheon Expressway in Korea during the same month were both attributed to the presence of BLACK-ICE [8]. Consequently, incidents resulting in casualties from BLACK-ICE accidents persist on a global scale. Various preventive measures, including the proposal of initiatives such as the installation of grooving, the deployment of LED signs, and the implementation of heat wires on road surfaces [15], are currently under consideration. However, given that these proposed measures are not preemptive, efforts are underway to formulate a proactive strategy aimed at preventing BLACK-ICE accidents. Identifying BLACK-ICE is challenging for drivers, creating perilous situations [8]. It is essential to anticipate, detect, and prevent BLACK-ICE formation, particularly for those managing winter road maintenance. Even though some advanced sensors exist for BLACK-ICE detection, they

TABLE I
SUMMARY OF EXISTING SENSOR DEVICES USED IN BLACK-ICE DETECTION.

Sensor Name	BLACK-ICE Detection Method	Main Challenge
Contact sensors [6], [7]	Temperature and humidity estimations to verify conditions conducive to black ice formation	Complexity of managing distributed sensors Substantial installation costs
Cameras [8], [9]	Vision-based approach to detect black ice on road surfaces	Susceptibility to low light conditions
IR sensors [10], [11] Optical sensors [12], [13]	Leveraging absorption coefficients that vary with wavelength	Susceptibility to sunlight interference

have some limitations. Table I illustrates a compilation of prevalent sensors utilized for ice detection, accompanied by their respective detection methodologies and associated challenges. Among these sensors, The most common sensor is the camera. While camera, vision base model for detecting, sensitivity to low-light conditions holds significance within the solution domain, it is noteworthy that in our application, deployed on CCTVs, the impact of low light conditions is mitigated.

This paper introduces an innovative method with significant potential as a cost-effective and tolerant solution applicable to diverse cold-climate scenarios where the detection of black ice formation holds paramount importance. In this regard, a Fully Convolutional Neural Network (FCNN) is utilized to extract the Region Of Interest (ROI) mask by detecting the road surface. Employing the resultant ROI as the input for the classifier markedly reduces computational load, concurrently elevating accuracy. After identifying the ROI geometry, a MobileNet classification model is employed to classify images as ICE or NOT-ICE, with BLACK-ICE falling under the ICE category. MobileNet represents an innovative convolutional neural network (CNN) architecture, acknowledged for its significance in deploying deep learning models on embedded devices with limited resources. Engineered to prioritize computational efficiency and robustness, MobileNet plays a crucial role in this study. To address specific misclassifications made by the MobileNet model, especially those involving BLACK-ICE images incorrectly categorized as NOT-ICE, our proposed model incorporates the α hyperparameter as a corrective criterion. The empirical findings in our investigation reveal the capacity to identify BLACK-ICE with a precision rate of 98.6%, a Process Time (PT) for one frame is 10.8 milliseconds, and a power consumption of 10.23 watts. These results underscore the efficacy of our algorithm in achieving real-time and dependable BLACK-ICE detection, particularly when deployed on edge devices.

II. PRELIMINARIES AND BACKGROUND

We have explored presenting our approach for classifying surfaces as ICE or NOT-ICE. We can effectively categorize images as ICE or NOT-ICE utilizing MobileNet. Subsequently, by leveraging sharpness and glossy factors, we can quantify the likelihood of BLACK-ICED surfaces in The HSV format if the classifier model's output is ICE.

A. HSV Image Format

The HSV color space is an alternative representation of images that separates color information into Hue, Saturation, and Value components. Unlike the RGB (Red, Green, Blue) color space, which is based on the primary colors of light, the HSV model is designed to mimic human's interpretation of colors. Hue represents the type of color, such as red, green, or blue. It is measured in degrees on a color wheel, where 0 and 360 correspond to red, 120 to green, and 240 to blue. The circular nature of the hue scale reflects the continuous spectrum of colors. Saturation refers to the intensity or vividness of a color. A saturation value of 0 results in a grayscale image, while higher values represent more vibrant colors. Saturation is typically normalized to a scale between 0 and 1. The value represents the brightness or lightness of a color. The 0 value corresponds to black, and 1 corresponds to white. Intermediate values determine the intensity of the color.

B. Sharpness and Glossiness

Sharpness refers to the clarity and detail in an image [16]. A sharp image has well-defined edges and fine details. Sharpness can be influenced by the quality of the camera, the focus accuracy, and the image resolution. High-resolution images captured with good optics and proper focus tend to appear sharper.

Glossiness refers to the perception of shininess or reflective quality in an image [17]. It is the property of a surface to reflect light in a specular (mirror-like) manner. Glossiness is often associated with the material and lighting conditions in a scene. Surfaces with high specular reflection, like polished metal or glass, appear glossy. The lighting setup plays a crucial role in emphasizing glossiness.

C. MobileNet

MobileNet is a family of neural network architectures designed for efficient and lightweight deep learning on mobile and embedded devices [18]. It was introduced by Google researchers in 2017 to address the computational constraints of deploying large and complex neural networks on devices with limited resources. The key innovation in MobileNet is the use of depthwise separable convolutions, which significantly reduces the number of parameters and computations while preserving the ability to capture meaningful features in the data.

Depthwise separable convolutions consist of two steps: depthwise convolutions and pointwise convolutions. In traditional convolutions, each filter processes the entire input volume, leading to a high computational cost. In contrast, depthwise separable convolutions apply a separate convolutional operation for each channel in the input (depthwise convolution) and then use a 1×1 convolution (pointwise convolution) to combine the outputs. This reduces the number of computations and, consequently, the model size. The MobileNet architecture is flexible and can be customized to different computational budgets by adjusting hyperparameters. This adaptability makes it suitable for different applications, including image classification, object detection, and semantic segmentation, particularly in scenarios where computational resources are limited, such as mobile phones, edge devices, and IoT devices. MobileNet has several versions, including MobileNet-V1, MobileNet-V2, and MobileNet-V3, each introducing improvements in terms of accuracy and efficiency. These models have become popular choices in computer vision for real-time applications on resource-constrained platforms.

D. Road Segmentation

Advanced driver assistance systems (ADAS) and automated driving systems (ADS) have attracted considerable scientific attention in recent years [19]. Road segmentation, one of the crucial modules, assesses the environment, finds the drivable area, and creates an occupancy map. A linked section of road surface that is free of automobiles, people, or other obstructions is known as a drivable region. Road segmentation supports other perception modules in the ADS workflow and produces an occupancy map for planning modules. As a result, precise and effective road segmentation is required [20]. Since cameras commonly provide high-resolution frames and are affordable, camera-based road segmentation has been studied for decades. For road segmentation, conventional computer vision algorithms used manually set characteristics like edges and histograms. However, those capabilities were difficult to adapt to new contexts and only operated in a few specific circumstances. In recent years, research has been more interested in algorithms based on CNNs. CNNs may handle a variety of driving circumstances by incorporating large convolutional kernels into a deep neural network. The precise drivable zone was produced using existing CNN-based road segmentation algorithms, including FCNN [21], SegNet [22], and StixelNet [23], but they were computationally expensive.

III. Proposed Method

In this section, the architectural design and details of the proposed method are elaborated. This section also presents the technical information regarding our image processing and model training. In pursuit of black ice detection, our approach unfolds in two distinct phases, delineated by the objectives of ROI mask determination and final decision-making.

A. The First Phase

This phase consists of the ROI mask determination which occurs as a one-time process for each CCTV system, maintaining a fixed viewpoint. To this end, we employed an FCNN [21] which represents an adapted model based on CNN, renowned for its efficacy in image classification. FCNN demonstrates proficiency in learning to delineate the road surface area within input images [5]. Comprising three segments including an encoder (consisting of a pre-trained model and 1-by-1 convolutions) and a decoder (involving transposed convolutions), FCNN exhibits notable performance. In our implementation, the VGG16 trained on the ImageNet dataset serves as the encoder. Notably, its 1-by-1 convolution layer is substituted with a fully-connected layer. The decoder incorporates transposed convolution layers to upsample the input, restoring it to its original size.

Figure 1(a) presents the input image. We denote it by $x \subset \mathcal{N}^{C \times H \times W}$, where C, H, and W indicate the number of input channels as well as the image height and width, respectively. The FCNN extracts the ROI identifying the road surface, as shown in Fig.1(b). Following this, Fig.1(c) presents its corresponding ROI mask M. Through the cropping of the input image using M, a masked image $x' \subseteq x$ is produced. Also, M remains constant for each CCTV system, computed only once and stored in the embedded memory. During the inference phase, it is retrieved from the memory, incurring no computational load. In addition, ROI acts to narrow down the processing area, optimizing the search for a solution and concurrently reducing overall power consumption. The focused processing not only minimizes PT, moving towards real-time problem-solving but also contributes to efficiency gains by excluding irrelevant points from processing, ultimately leading to a reduction in overall power consumption.

B. The Second Phase

The primary objective of this phase is to detect the BLACK-ICE while enhancing the performance and concurrently reducing energy consumption and resource utilization compared to contemporary methods. In this regard, this section delineates our algorithm and the implementation for calculating the likelihood of the existence of BLACK-ICE in the masked image x'. Initially, we constructed a dataset comprising road surface images, categorized into two classes: ICE and NOT-ICE. In this classification, images containing BLACK-ICE are designated under the ICE category. For the classification of the input image x', we conduct training on the MobileNet-V2 model [24] using our generated dataset which generates from [25] dataset images. This model predicts the likelihood of x' for the ICE class, denoted as $y_{ice} \in [0, 1]$, and can be parameterized as Equation (1).

$$y_{ice} = \mathcal{M}(\Theta, x') \tag{1}$$

where, $\mathcal{M}$ is tne computational mode (MobileNet-v2) and Θ is the model parameters. Of course, for each input image x', the MobileNet-v2 generates two values $y_{ice}, \bar{y}_{ice} \epsilon [0, 1]$, which represent the ICE likelihood and NOT-ICE likelihood, respectively. Since $y_{ice} + \bar{y}_{ice} = 1$, we omit $\bar{y}_{ice}$ in the presentation.

(a) The input image x.

(b) Overlaying the ROI mask M with x.

(c) The masked ROI x'.

Fig. 1. The steps of generating ROI by the FCNN model.

Then, the sharpness factor $\mathcal{S}$ [26] of x' is calculated according to the gradient of the image by Equation (2).

$$\mathcal{S} = \frac{1}{|x'|} \sum_{i \in x'} \sqrt{\left(\frac{\partial \mathcal{I}_i}{\partial w_i}\right)^2 + \left(\frac{\partial \mathcal{I}_i}{\partial h_i}\right)^2} \tag{2}$$

where, $|x'|$ is the total number of pixels in x', $\mathcal{I}_i \in [0, 255]$ indicates the intensity of the pixel i, and (w_i, h_i) is its position in the image x'. As well, the intensity $\mathcal{I}_i$ for each pixel i of an HSV image is approximately calculated by Equation (3), where H_i, S_i and V_i are the corresponding Hue, Saturation, and Value parameters, respectively.

$$\mathcal{I}_i \simeq 0.299 \times H_i + 0.587 \times S_i + 0.114 \times V_i \tag{3}$$

In Equation (2) the $\frac{\partial \mathcal{I}_i}{\partial w_i}$ and $\frac{\partial \mathcal{I}_i}{\partial h_i}$ are the partial derivatives of intensity with respect to w_i and h_i, representing the gradients in the horizontal and vertical directions. The glossiness is intricately linked to the manner in which light interacts with the surfaces depicted in an image. In the endeavor to quantify glossiness, we engage in the computation of local contrast. This process entails determining the standard deviation of pixel intensities within defined localized regions, thereby serving as a metric for assessing contrast. The glossiness factor g_i [27] of pixel i located in (w_i, h_i) position can be estimated utilizing Equation (4).

$$g_i = \sqrt{\frac{1}{|N_i|} \sum_{j \in N_i} \left(\mathcal{I}_j - \bar{\mathcal{I}}_i\right)^2} \tag{4}$$

where, N_i denotes the set of neighboring pixels of pixel i, $\mathcal{I}_j$ represents the intensity of the pixel situated at the position (w_j, h_j) in the image x'. Also, $\bar{\mathcal{I}}_i$ signifies the average intensity of all the pixels in N_i. The comprehensive glossiness factor for an entire image can be approximated through Equation (5).

$$\mathcal{G} \simeq \mathbb{E}_{\ i \in x'}\left[g_i\right] \tag{5}$$

For the computation of Sharpness and Glossiness factors $\mathcal{S}$ and $\mathcal{G}$, the HSV representation of the input image x' is employed. This choice was motivated by the inherent advantages of HSV, where the manipulation of overall image brightness while preserving color information is more straightforward compared to the RGB representation. As delineated by Equations (1) to (5), the parameters $\mathcal{G}$, $\mathcal{S}$, and y_{ice} exhibit mutual independence, enabling concurrent computation during the inference phase. At the end, the detection of differences between ICE and BLACK-ICE is achieved through the multiplication of $\mathcal{G}$ and $\mathcal{S}$ which denote as ω and calculate from equation 6, while the identification of NOT-ICE, representing a normal road surface, is facilitated by the presence of y_{ice}.

$$\omega = \mathcal{G} \times \mathcal{S} \tag{6}$$

We have introduced a novel equation to calculate a unique parameter known as the BLACK-ICE Factor, expressed in Equation 9. In Equation 9, the parameter ν and μ are computed using Equation 7, 8 where α and φ represent the hyperparameter. Additionally, $\wedge$ corresponds to the logical "and" operation.

$$\nu = \begin{cases} 0 & if \quad y_{ice} < \alpha \\ 1 & if \quad y_{ice} \geq \alpha \end{cases} \tag{7}$$

$$\mu = \begin{cases} 0 & if \quad \omega < \varphi \\ 1 & if \quad \omega \geq \varphi \end{cases} \tag{8}$$

$$\mathcal{B} = \mu \wedge \nu \tag{9}$$

Figure 2 illustrates three categories of road surfaces in RGB format as well as their corresponding HSV images. The values of $\mathcal{G}$, $\mathcal{S}$, ω and y_{ice} as well as the corresponding BLACK-ICE Factor $\mathcal{B}$ for the HSV images are detailed in Table II. Significantly, the average value of ω for 100 images classified as BLACK-ICE is $\mathbf{1719.12}$, demonstrated as AVG_{BI}. Also, this average for 100 ICE images that are not BLACK-ICE is $\mathbf{118.81}$, demonstrated as AVG_{WI}. The difference between AVG_{BI} and AVG_{WI} provides a reasonable basis to conclude that if ω exceeds the threshold of 1000, the model classifies x' as BLACK-ICE, suggesting that setting φ to 1000 is advisable. Algorithm 1 presents the general procedure of our proposed model.

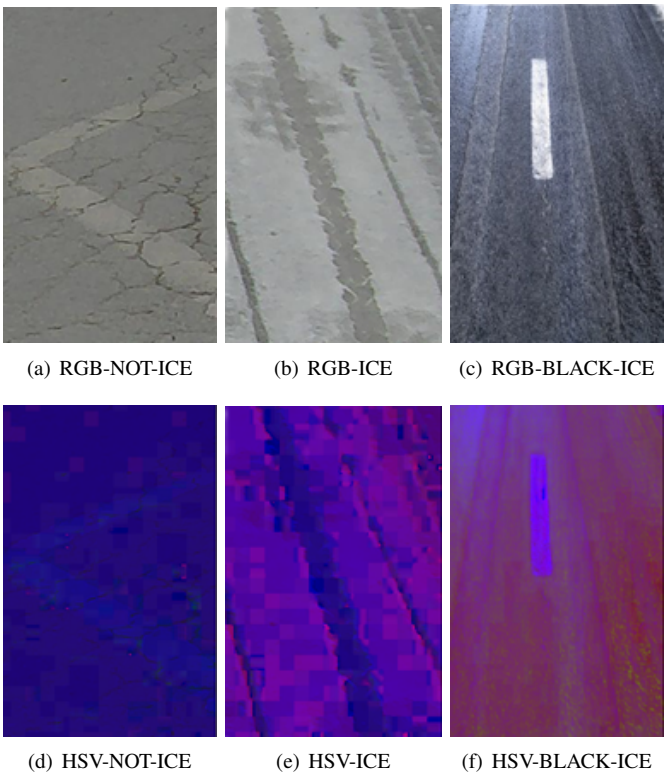

(a) RGB-NOT-ICE (b) RGB-ICE (c) RGB-BLACK-ICE

(d) HSV-NOT-ICE (e) HSV-ICE (f) HSV-BLACK-ICE

Fig. 2. Three road surfaces in RGB format with their corresponding HSV format.

TABLE II
THE VALUES OF $\mathcal{G}$, $\mathcal{S}$, y_{ice}, AND $\mathcal{B}$ FOR FIG.2 IMAGE AS WELL AS AVG_{BI} AND AVG_{WI} REPRESENT THE AVERAGE OF THE PARAMETERS FOR 100 IMAGES FOR BLACK-ICE AND ICE (NOT BLACK-ICE) CATEGORIES.

Category	$\mathcal{S}$	$\mathcal{G}$	y_{ice}	ω	$\mathcal{B}$
BLACK-ICE	25.34	84.76	0.84	2147.81	1
ICE	4.97	14.85	0.96	73.80	0
NOT-ICE	20.24	8.49	0.13	171.83	0
AVG_{BI}	27.21	63.18	0.85	1719.12	1
AVG_{WI}	6.77	17.55	0.93	118.81	0

Algorithm 1 BLACK-ICE Detection.

Inputs: x (Input image), M (ROI mask), Θ (MobileNet parameters), α and φ (hyperparameters)
Output: BLACK-ICE existence label
$x' \leftarrow M(x)$
begin parallel_section
  $y_{ice} \leftarrow \mathcal{M}(\Theta, x')$
  $\mathcal{S} \leftarrow$ Equation 2
  $\mathcal{G} \leftarrow$ Equation 5
end parallel_section
$\omega \leftarrow Equation6$
$\nu \leftarrow Equation7$
$\mu \leftarrow Equation8$
$\mathcal{B} \leftarrow Equation9$
if $\mathcal{B} == 0$ **then**
  return Not BLACK-ICE
else
  return "BLACK-ICE"
end

IV. EVALUATION AND DISCUSSION

This section assesses our suggested approach and contrasts it with the most effective state-of-the-art approaches. The proposed algorithm is implemented and executed on a Mini-PC Intel® NUC Core™ i5-1145G7 Processor with 8 MB Cache, 16 GB DDR4 RAM, and 4.4 GHz frequency.

A. Experimental Setup

In the initial phase of our experimentation, we first train the FCNN model to acquire the road mask, denoted as M. This mask is subsequently stored in embedded memory for the inference phase. The training process involved utilizing the KITTI Road dataset [28], comprising 508 images designed for road and lane estimation. These images were formatted in a bird's-eye-view perspective, with a resolution of 128×128 pixels. Specifically, 384 images were designated for the training section, while the remaining 124 images constituted the test set. The FCNN underwent training with 100 epochs, a batch size of 8, and a learning rate of 0.001, ultimately achieving a commendable test accuracy of 87.3%.

In the subsequent step, we trained the MobileNet-v2 model parameters, Θ, according to the hyperparameters detailed in Table IV and the datasets presented in [25]. The distribution of images in each category is outlined in Table III and the BLACK-ICE images are encompassed within the ICE category. The MobileNet model demonstrated a high accuracy of 97.8% in classifying ICE and NOT-ICE images on the test images.

The proposed algorithm underwent rigorous testing on three types of datasets which we refer to as *TYPE I*, *TYPE II*, and *TYPE III*. Besides, *TYPE I* comprises 50 ICE images and 20 BLACK-ICE images, serving the sole purpose of assessing the accuracy in detecting BLACK-ICE from ICE images through the utilization of glossiness and sharpness factors. Also, *TYPE II* consists of 50 ICE images, 20 BLACK-ICE images, and an additional 80 NOT-ICE images, aimed to evaluate the accuracy and PT of BLACK-ICE detection using MobileNet and BLACK-ICE factor $\mathcal{B}$. Additionally, *TYPE III* mirrors the image quantity and category distribution of *TYPE II*, differs in that the images contain additional details beyond the road surface for analyzing the effects of M on the accuracy, PT, and power usage. *TYPE III* is employed to gauge the accuracy and PT of the proposed algorithm outlined in Algorithm 1. For *TYPE III* dataset, a road surface mask M was computed and stored for each image. Subsequently, in the ensuing subsection, we compare the accuracy and power usage of our proposed algorithm with other vision-based models, ultimately reporting on the observed PT.

TABLE III
GENERATED DATASET FOR TRAINING THE MOBILNET-V2 MODEL. BLACK-ICE IMAGES ARE ENCOMPASSED WITHIN THE ICE CATEGORY.

Category	*# Train*	*# Test*
ICE	250	50
BLACK-ICE	70	10
NOT-ICE	320	60

TABLE IV
THE HYPERPARAMETERS OF MOBILENET-V2.

Hyperparameter	***Value***
Width Multiplier	1.0
Resolution Multiplier	1.0
Depthwise Separable Convolution	Yes
Initial Number of Filters	32
Expansion Factor	6
Dropout Rate	0.2
Activation Function	ReLU
Number of Classes	2
Batch Size	16
Number of Epochs	100

B. Discussion

In this section, we conduct a comparative evaluation of the model accuracy (ACC) and processing time (PT) across the test dataset. As illustrated in Fig.3, the best value for α is determined to be 0.3. Additionally, in accordance with the recommendation provided at the conclusion of Section III-B, it is advisable to set the value of φ to 1000. The outcomes presented in Table V indicate that the proposed model attains a perfect accuracy of 100% in detecting BLACK-ICE in *TYPE I*. In *TYPE II*, the proposed model achieves an accuracy of 98.9%. As indicated in Table V, the accuracy of our proposed model in detecting BLACK-ICE surpasses that of the MobileNet-V2 model (97.8%). This improvement is attributed to cases where BLACK-ICE images are potentially misclassified as NOT-ICE by MobileNet-V2. Our proposed algorithm (1) addresses this by detecting such images through the calculation of the BLACK-ICE factor,$\mathcal{B}$. Additionally, it is worth noting that both *TYPE II* and *TYPE I* share identical PT values, thanks to the parallel processing section of the proposed algorithm, as detailed in Table V. Lastly, in *TYPE III*, the proposed model's accuracy experiences a slight decrease (98.6%) influenced by the incorporation of FCNN effects. Despite this decrease, the PT of the proposed algorithm is recorded at 10.8 ms, demonstrating appropriateness for real-time processing [29].

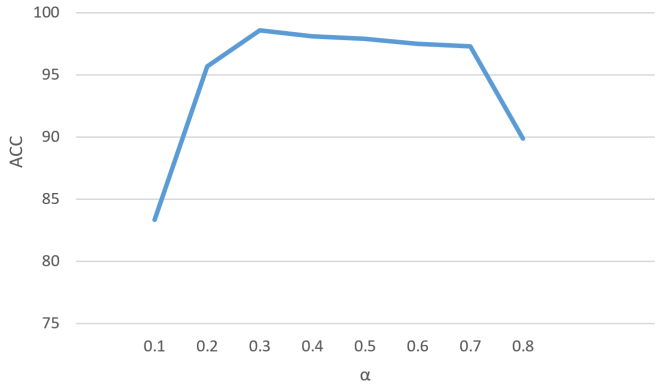

Fig. 3. The effect of α on the proposed model ACC on the *TYPE III* DATASET.

A further property of the presented model is power efficiency, in line with our overarching goal of functioning on resource-aware systems. To measure power usage, we employed the *cProfile Python* library. For the comparison, we calculated the number of MAC operations for both the proposed model and the other models, estimating their power usage based on the relationship between the number of MAC operations and power. As delineated in Table VI, the proposed model demonstrates the most economical power consumption, registering at 10.23 W, compared to the other models under consideration. This observation underscores the suitability of the proposed model for operation on resource-aware devices. Moreover [8] attains the highest level of accuracy at an impressive 98.3%, yet our proposed model achieves 98.6% accuracy in detecting BLACK-ICE, demonstrating superior reliability compared to [8] and [30]. Additionally, considering the power usage of the proposed model is 33% less than that of [8], it exhibits better overall performance than these counterparts. This improvement becomes particularly critical when deploying the proposed model on edge devices such as CCTVs and portable devices with limited resources.

TABLE V
THE ACCURACY (ACC) AND PT OF ALGORITHM 1 ON DIFFERENT DATASETS.

TYPE	***ACC%***	***PT(ms)***
I	100	9.1
II	98.9	9.1
III	98.6	10.8

TABLE VI
COMPARISON OF THE POWER CONSUMPTION AND ACCURACY OF THE PROPOSED MODEL WITH OTHER VISION BASE MODELS ON *TYPE III* DATASET.

Model	***Power(W)***	***ACC%***
Proposed model	**10.23**	**98.6**
CNN [30]	13.52	95.6
CNN [8]	15.31	98.3
Hyperspectral Imaging [31]	12.78	97
Image Analysis [32]	10.83	95
Image Analysis [33]	9.74	83

V. RELATED WORKS

The identification of BLACK-ICE has been investigated through diverse approaches, encompassing sensor-based methods [34], [35], sound wave utilization [36], [37], and the application of light sources [38]. Tabatabai and Aljuboori [34] focused on BLACK-ICE, ice, and water detection on roads and bridges, employing sensors embedded within concrete. Their proposed sensor, based on alterations in electrical resistance between stainless steel columns inside the concrete, proved effective in detecting road surface conditions, offering potential for accident prevention.

Additionally, Alimasi et al [39] designed a BLACK-ICE detector using an optical sensor and an infrared thermometer. Abdalla et al [35] introduced a Kinect-based system for BLACK-ICE detection, including the classification of various ice types, thickness, and volume measurement. They achieved

high accuracy in distinguishing ice types within a specific camera range, with a low error rate in measured thickness and volume.

Ma and Ruan [38] investigated a BLACK-ICE detection method utilizing three-wavelength non-contact optical technology. Employing wavelengths (1310 nm, 1430 nm, 1550 nm), they differentiated dry, wet, BLACK-ICE, ice, and snowy conditions. Successfully detecting BLACK-ICE through the reflectance of each wavelength, their study laid the groundwork for potential equipment development in road condition detection.

Kim et al [30] utilized Range-FFT results obtained by the mmWave sensor for BLACK-ICE detection, with accuracy dependent on the surface's smoothness or roughness. Furthermore, Lee et al [8] employed CNNs for BLACK-ICE detection using camera images. Despite achieving high accuracy through deep learning, this approach incurred increased computational operations and subsequent higher power consumption.

VI. Conclusion

The primary objective of this research is the development of an efficient algorithm for BLACK-ICE detection in CCTV images, emphasizing considerations of accuracy and resource efficiency tailored for edge devices. At first, an FCNN generates the ROI mask according to each camera view, emphasizing the road surface. This strategy reduces computational load and diminishes power consumption when executing on resource-aware edge devices. In the following, a MobileNet-V2 model is trained to classify the ROI region into either ICE or NOT-ICE categories. Simultaneously, Glossiness and Sharpness factors are computed for this region. In addition, we introduced a BLACK-ICE factor ($\mathcal{B}$) based on the Glossiness, Sharpness, and ICE likelihood calculated by the MobileNet model to identify instances of BLACK-ICE. The presented algorithm showcased an accuracy level of 98.6% with a power consumption of 10.23 W, reflecting a significant reduction of 33% in power usage and superior accuracy in comparison to current vision-based models. This comprehensive approach integrates multiple image analysis techniques, contributing to a robust solution for real-time BLACK-ICE detection in surveillance scenarios.

Acknowledgment

This research was supported by the Brain Pool program funded by the Ministry of Science and ICT through the National Research Foundation of Korea (NRF-2021H1D3A2A02040040) and in part supported by the Basic Science Research Program through the National Research Foundation of Korea (NRF) funded by the Ministry of Education (NRF-2020R1I1A3063857).

References

[1] V. Wiley, T. Lucas, Computer vision and image processing: a paper review, International Journal of Artificial Intelligence Research 2 (1) (2018) 29–36.

[2] T.-W. Seo, S.-R. Lee, B.-C. Bae, E. Yoon, C.-S. Kim, et al., An analysis of vulnerabilities and performance on the cctv security monitoring and control, Journal of Korea Multimedia Society 15 (1) (2012) 93–100.

[3] A. C. Davies, S. A. Velastin, A progress review of intelligent cctv surveillance systems, Proc. IEEE IDAACS (2005) 417–423.

[4] M. P. Ashby, The value of cctv surveillance cameras as an investigative tool: An empirical analysis, European Journal on Criminal Policy and Research 23 (3) (2017) 441–459.

[5] N. Mohammadreza, S. Gorgin, D. Javaheri, J.-A. Lee, Ice detection on edge device based on most significant digit first svm, in: Proceedings of the 2022 6th International Conference on Video and Image Processing, 2022, pp. 61–66.

[6] T. Liu, Q. Pan, J. Sanchez, S. Sun, N. Wang, H. Yu, Prototype decision support system for black ice detection and road closure control, IEEE Intelligent Transportation Systems Magazine 9 (2) (2017) 91–102.

[7] H. Tabatabai, M. Aljuboori, A novel concrete-based sensor for detection of ice and water on roads and bridges, Sensors 17 (12) (2017) 2912.

[8] H. Lee, M. Kang, J. Song, K. Hwang, The detection of black ice accidents for preventative automated vehicles using convolutional neural networks, Electronics 9 (12) (2020) 2178.

[9] C. H. Crawford, S. Daijavad, J. A. Gunnels, T. Nowicki, G. M. Swirszcz, J. Xenidis, Method for black ice detection and prediction, uS Patent 9,940,549 (Apr. 10 2018).

[10] P. Jonsson, Remote sensor for winter road surface status detection, in: SENSORS, 2011 IEEE, IEEE, 2011, pp. 1285–1288.

[11] Y. Nakanishi, Y. Kushihi, Black-ice and standing-water detection system, uS Patent App. 16/647,046 (Dec. 2 2021).

[12] N. ALIMASI, S. TAKAHASHI, H. ENOMOTO, Development of a mobile optical system to detect road-freezing conditions, Bulletin of Glaciological Research 30 (2012) 41–51.

[13] X. Ma, C. Ruan, Method for black ice detection on roads using tri-wavelength backscattering measurements, Applied Optics 59 (24) (2020) 7242–7246.

[14] Snow & ice road weather management [accessed 29-11-2023], `https://ops.fhwa.dot.gov/weather`.

[15] A. Abdelaal, M. Sarayloo, D. K. Nims, B. Mohammadian, J. Heil, H. Sojoudi, A flexible surface-mountable sensor for ice detection and non-destructive measurement of liquid water content in snow, Cold Regions Science and Technology 195 (2022) 103469.

[16] D. Shaked, I. Tastl, Sharpness measure: Towards automatic image enhancement, in: IEEE International Conference on Image Processing 2005, Vol. 1, IEEE, 2005, pp. I–937.

[17] A. C. Chadwick, R. Kentridge, The perception of gloss: A review, Vision research 109 (2015) 221–235.

[18] A. G. Howard, M. Zhu, B. Chen, D. Kalenichenko, W. Wang, T. Weyand, M. Andreetto, H. Adam, Mobilenets: Efficient convolutional neural networks for mobile vision applications, arXiv preprint arXiv:1704.04861 (2017).

[19] A. Shaout, D. Colella, S. Awad, Advanced driver assistance systems-past, present and future, in: 2011 Seventh International Computer Engineering Conference (ICENCO'2011), IEEE, 2011, pp. 72–82.

[20] R. Matthaei, B. Lichte, M. Maurer, Robust grid-based road detection for adas and autonomous vehicles in urban environments, in: Proceedings of the 16th International Conference on Information Fusion, IEEE, 2013, pp. 938–944.

[21] J. Long, E. Shelhamer, T. Darrell, Fully convolutional networks for semantic segmentation, in: Proceedings of the IEEE conference on computer vision and pattern recognition, 2015, pp. 3431–3440.

[22] V. Badrinarayanan, A. Kendall, R. Cipolla, Segnet: A deep convolutional encoder-decoder architecture for image segmentation, IEEE Transactions on Pattern Analysis and Machine Intelligence 39 (12) (2017) 2481–2495.

[23] D. Levi, N. Garnett, E. Fetaya, I. Herzlyia, Stixelnet: A deep convolutional network for obstacle detection and road segmentation., in: BMVC, Vol. 1, 2015, p. 4.

[24] M. Sandler, A. Howard, M. Zhu, A. Zhmoginov, L.-C. Chen, Mobilenetv2: Inverted residuals and linear bottlenecks, in: Proceedings of the IEEE conference on computer vision and pattern recognition, 2018, pp. 4510–4520.

[25] T. Zhao, Y. Wei, Road surface image dataset with detailed annotations (2022). doi:10.17632/w86hvkrzc5.2.

[26] C. Feichtenhofer, H. Fassold, P. Schallauer, A perceptual image sharpness metric based on local edge gradient analysis, IEEE Signal Processing Letters 20 (4) (2013) 379–382.

[27] H. KUGISAWA, T. AIDA, M. EBATA, Method for measuring glossiness of spherical surfaces utilizing brightness pattern of image, IEICE Transactions on Fundamentals of Electronics, Communications and Computer Sciences 74 (9) (1991) 2655–2662.

[28] J. Fritsch, T. Kuehnl, A. Geiger, A new performance measure and evaluation benchmark for road detection algorithms, in: International Conference on Intelligent Transportation Systems (ITSC), 2013.
[29] Z. Chen, W. Hu, J. Wang, S. Zhao, B. Amos, G. Wu, K. Ha, K. Elgazzar, P. Pillai, R. Klatzky, et al., An empirical study of latency in an emerging class of edge computing applications for wearable cognitive assistance, in: Proceedings of the Second ACM/IEEE Symposium on Edge Computing, 2017, pp. 1–14.
[30] J. Kim, E. Kim, D. Kim, A black ice detection method based on 1-dimensional cnn using mmwave sensor backscattering, Remote Sensing 14 (20) (2022) 5252.
[31] C. Bhattacharyya, S. Kim, Black ice classification with hyperspectral imaging and deep learning, Applied Sciences 13 (21) (2023) 11977.
[32] M. Ahmad, A. M. Khan, M. Mazzara, S. Distefano, M. Ali, M. S. Sarfraz, A fast and compact 3-d cnn for hyperspectral image classification, IEEE Geoscience and Remote Sensing Letters 19 (2022) 1–5. doi:10.1109/LGRS.2020.3043710.
[33]
[34] H. Tabatabai, M. Aljuboori, A novel concrete-based sensor for detection of ice and water on roads and bridges, Sensors 17 (12) (2017) 2912.
[35] Y. E. Abdalla, M. T. Iqbal, M. Shehata, Black ice detection system using kinect, in: 2017 IEEE 30th Canadian Conference on Electrical and Computer Engineering (CCECE), IEEE, 2017, pp. 1–4.
[36] R. Minullin, R. Mustafin, Y. V. Piskovatskii, S. Vedernikov, I. Lavrent'Ev, A detection technique for black ice and frost depositions on wires of a power transmission line by location sounding, Russian Electrical Engineering 82 (10) (2011) 541–543.
[37] D. Gailius, S. Jačėnas, Ice detection on a road by analyzing tire to road friction ultrasonic noise, Ultragarsas/Ultrasound 62 (2) (2007) 17–20.
[38] X. Ma, C. Ruan, Method for black ice detection on roads using tri-wavelength backscattering measurements, Applied Optics 59 (24) (2020) 7242–7246.
[39] N. ALIMASI, S. TAKAHASHI, H. ENOMOTO, Development of a mobile optical system to detect road-freezing conditions, Bulletin of Glaciological Research 30 (2012) 41–51.